Influence of human amylin on the membrane stability of rat primary hippocampal neurons

Nan Zhang[1,2], Yuan Xing[3,4], Yongzhou Yu[5], Chao Liu[6], Baohua Jin[5], Lifang Huo[5], Dezhi Kong[5], Zuxiao Yang[5], Xiangjian Zhang[7], Ruimao Zheng[8], Zhanfeng Jia[9], Lin Kang[10], Wei Zhang[5]

[1]Central Laboratory, First Hospital of Hebei Medical University, Shijiazhuang, Hebei, China
[2]Hebei International Joint Research Center for Brain Science, Shijiazhuang, Hebei, China
[3]Department of Neurology, First Hospital of Hebei Medical University, Shijiazhuang, Hebei, China
[4]Brain Aging and Cognitive Neuroscience Key Laboratory of Hebei Province, Shijiazhuang, Hebei, China
[5]Department of Pharmacology, Institution of Chinese Integrative Medicine, Hebei Medical University, Shijiazhuang, Hebei, China
[6]Department of Laboratory Animal Science, Hebei Medical University, Hebei Key Lab of Laboratory Animal Science, Shijiazhuang, Hebei, China
[7]Hebei Key Laboratory of Vascular Homeostasis and Hebei Collaborative Innovation Center for Cardio-Cerebrovascular Disease, Department of Neurology, Second Hospital of Hebei Medical University, Shijiazhuang, Hebei, China
[8]Department of Anatomy, Histology and Embryology, Health Science Center, Neuroscience Research Institute, Key Laboratory for Neuroscience of the Ministry of Education, Key Laboratory for Neuroscience of the National Health Commission, Peking University, Beijing, China
[9]Department of Pharmacology, The Key Laboratory of New Drug Pharmacology and Toxicology, Center for Innovative Drug Research and Evaluation, Institute of Medical Science and Health, The Key Laboratory of Neural and Vascular Biology Ministry of Education, Hebei Medical University, Shijiazhuang, Hebei, China
[10]Department of Endocrinology, The Second Clinical Medical College of Jinan University, Shenzhen People's Hospital, Clinical Medical Research Center, The First Affiliated Hospital of Southern University of Science and Technology, Shenzhen, China

ABSTRACT

The two most common aging-related diseases, Alzheimer's disease and type 2 diabetes mellitus, are associated with accumulation of amyloid proteins (β-amyloid and amylin, respectively). This amylin aggregation is reportedly cytotoxic to neurons. We found that aggregation of human amylin (hAmylin) induced neuronal apoptosis without obvious microglial infiltration *in vivo*. High concentrations of hAmylin irreversibly aggregated on the surface of the neuronal plasma membrane. Long-term incubation with hAmylin induced morphological changes in neurons. Moreover, hAmylin permeabilized the neuronal membrane within 1 min in a manner similar to Triton X-100, allowing impermeable fluorescent antibodies to enter the neurons and stain intracellular antigens. hAmylin also permeabilized the cell membrane of astrocytes, though more slowly. Under scanning electron microscopy, we observed that hAmylin destroyed the integrity of the cell membranes of both neurons and astrocytes. Additionally, it increased intracellular reactive oxygen species generation and reduced the mitochondrial membrane potential. Thus, by aggregating on the surface of neurons, hAmylin impaired the cell membrane integrity, induced reactive oxygen species production, reduced the mitochondrial membrane potential, and ultimately induced neuronal apoptosis.

INTRODUCTION

Alzheimer's disease and type 2 diabetes mellitus (DM2) are the most common aging-related diseases [1, 2]. Multiple studies have indicated that there is a strong correlation between these two diseases, and about 80% of Alzheimer's disease patients are estimated to have an impaired glucose tolerance or DM2 [3]. Protein aggregation has been linked to the pathogenesis of aging-related degenerative diseases [4]. For example, Alzheimer's disease is characterized by β-amyloid accumulation [1]. On the other hand, amylin aggregation causes pancreatic β-cell damage and insulin deficiency, which are components of the pathogenesis of DM2 [5]. Like β-amyloid, human amylin (hAmylin) tends to misfold into toxic structures and form amyloid deposits [6, 7] as protein degradation decreases with aging [4].

The aggregation of hAmylin has been reported to impair the integrity and alter the permeability of the cell membrane [9–11]. The negative charges on the surface of the phospholipid bilayer facilitate the insertion of positively charged hAmylin. Mirzabekov [12] reported that 1-10 μM hAmylin formed non-selective ion channels that were permeable to Ca^{2+}, Na^+, K^+ and Cl^- on the plasma membranes of islet β-cells, and dose-dependently increased the electrical conductivity of the plasma membrane. Numerous other studies have indicated that hAmylin reduces the concentration of lipids in the cell membrane and forms non-selective ion channels during its aggregation on the membrane surface [17, 18]. Impaired cell membrane integrity alters the intracellular Ca^{2+} concentration ($[Ca^{2+}]_i$) and eventually induces endoplasmic reticulum stress and apoptosis. In the case of β-amyloid, oligomerization of this protein on the plasma membrane surface generates large amounts of reactive oxygen species (ROS) and thereby destroys the membrane stability [19, 20]. Although many studies have investigated the cytotoxicity of hAmylin, the mechanisms by which it induces membrane damage in different states (monomeric, oligomeric or fibrous) and induces cell death are still unclear.

The sequence of amylin determines its propensity to form amyloid fibrils. For example, rodent amylin differs from hAmylin by only six of its 37 residues, and yet does not form fibrils. Five of these six residues are located between residues 20 and 29, the region that is known to be important for hAmylin fibrillation [13]. Furthermore, three of the six residues are occupied by proline (at positions 25, 28 and 29), a well-known disrupter of secondary structures such as β-sheets. While rodents, dogs and cows do not form fibrils, primates, cats, pigs, ferrets and guinea pigs can form amyloid fibrils and are prone to DM2 [14, 15]. Potter [16] demonstrated that the ability of hAmylin to aggregate and damage the cell membranes of human islet cells *in vitro* depended on a sequence of 13-28 amino acids; thus, when this sequence was replaced, the survival rate of the islet cells significantly improved. These results suggested that hAmylin impairs the membrane integrity mainly by aggregating.

Oligomers and plaques of hAmylin have been identified not only in the pancreas, but also in the temporal lobe gray matter of diabetic patients, demonstrating the potential neurotoxicity of hAmylin [8]. In addition, hAmylin oligomer deposits have been detected in the brains of late-onset Alzheimer's disease patients [8, 24, 25], and have been reported to impair memory in rats [26]. We previously found that a brief application of hAmylin could activate the transient receptor potential vanilloid 4 channels (TRPV4, the non-selective cation channels that are sensitive to mechanical stimulation and osmotic pressure [21–23]) and increase the $[Ca^{2+}]_i$ in cultured hippocampal neurons [14]. Similar results have been observed in MIN6 cells [21]. Thus, we speculated that hAmylin damages neuronal cells and promotes neuronal sensitivity to other sources of damage.

In the present study, we assessed hAmylin aggregation in neurons and investigated its effects on cell membrane stability, ROS levels and the mitochondrial membrane potential (mtΔΨ).

RESULTS

hAmylin induced neuronal loss in hippocampal tissue *in vivo*

Previous studies have demonstrated that, similar to oligomeric β-amyloid, hAmylin is toxic to several kinds of cells *in vitro* [6, 27–29]. To determine the effects of hAmylin *in vivo*, we injected 5 μL of hAmylin (10 μM) into the right lateral ventricles of adult mice (Figure 1A). Terminal deoxynucleotidyl transferase dUTP nick end labeling (TUNEL) staining was used to detect neuronal apoptosis induced by hAmylin. Twenty-four hours after the injection, the proportion of apoptotic cells in the hippocampal dentate gyrus was significantly greater in the hAmylin group than in the control group (***p < 0.001, Figure 1B and 1C). Transmembrane protein 199 (TMEM199)[+] cells (microglia) and ionized calcium binding adaptor molecule 1 (Iba1)[+] cells (microglia and macrophages) were not observed (Supplementary Figure 1A and 1B), indicating that microglial migration was not involved and that neuronal cells were probably the main targets of hAmylin.

Aggregation of hAmylin on the surface of neurons

Next, we fluorescently labeled the N-terminus of hAmylin with fluorescein amidite (FAM), and investigated whether the peptide entered neurons. Consistent with our previous findings [14], FAM-hAmylin easily aggregated when it was incubated with primary cultured neurons at 37 °C for 30 min. Many fluorescent aggregates were observed under a microscope, and FAM-hAmylin aggregation slowly increased with increasing incubation times (Figure 2A and 2B). However, after the culture dishes were washed with fresh medium and shaken, most of the fluorescence representing aggregated hAmylin disappeared (Figure 2C), indicating that the aggregation process of hAmylin oligomers was irreversible, but the aggregates of hAmylin probably attached to the surface of the cell membrane instead of entering the neurons.

Long-term effects of hAmylin on the morphology of hippocampal neurons

Since hAmylin was able to aggregate on the surface of neurons, we used a live-cell imaging system to measure the effects of 10 μM hAmylin on neuronal survival over a long period of incubation. We used cell rupture as an indication of cell death (Figure 3A). Only 77.78% of neurons survived after being incubated with hAmylin for 12 h, while a significantly greater proportion of neurons survived in the control group (***p < 0.001, Figure 3B). We also used cellular immunofluorescence to detect the effects of hAmylin incubation on measures of cell morphology (Figure 3C and 3D), including cell size, neurite length, neurite number and synapse number (Figure 3E–3H, respectively). After the neurons had been incubated with 10 μM hAmylin for 4 h, their synapse numbers (***p < 0.001) and neurite lengths (*p < 0.05) were significantly reduced. After 9 h of incubation, the cell sizes (***p < 0.001) and neurite numbers (***p < 0.001) were significantly reduced.

Effects of hAmylin on the cell membrane integrity

It is well known that macromolecules such as primary antibodies cannot pass through the cell membrane unless it has been permeabilized, for instance, by Triton X-100. We took advantage of this property of antibodies in immunofluorescence experiments to
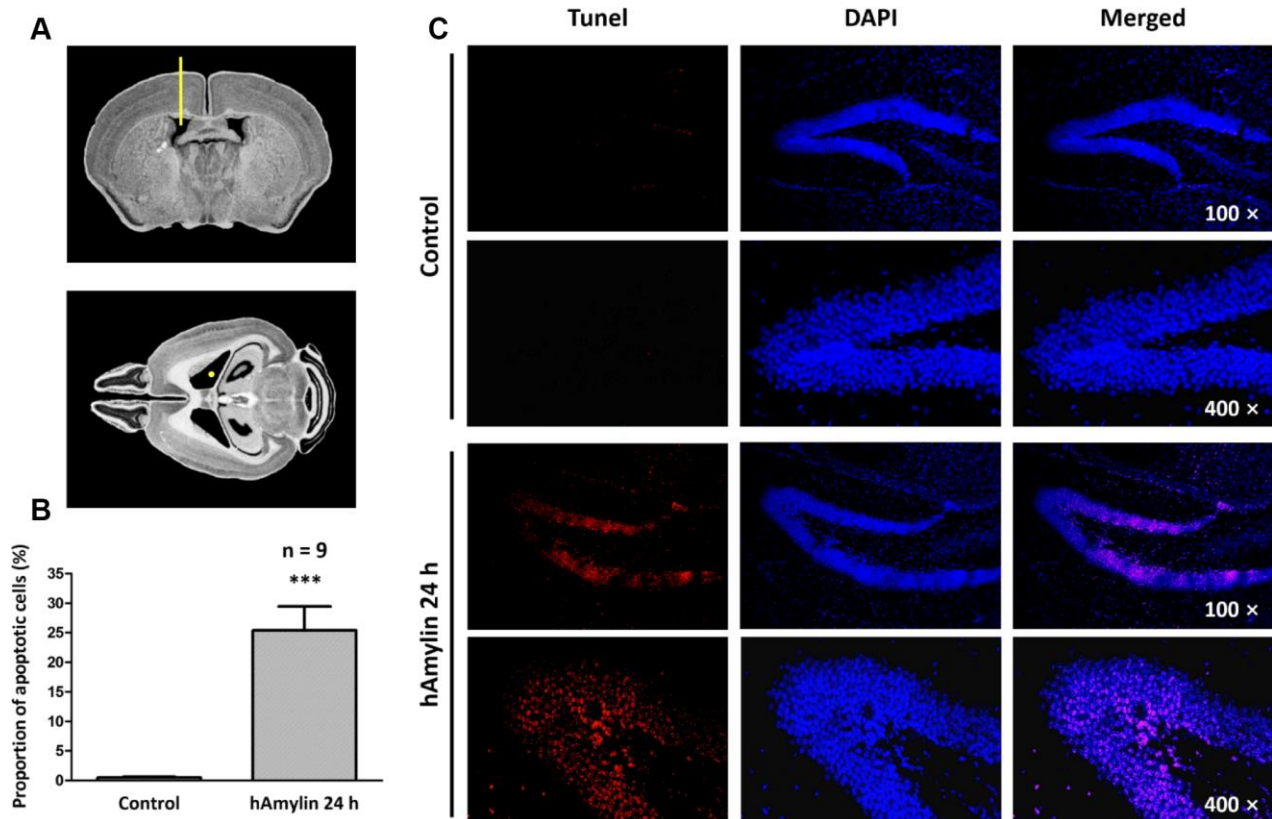

Figure 1. Immunostaining of hippocampal cells in brain slices from adult Kunming mice. (**A**) The right lateral ventricle was injected with 5 μL of hAmylin (10 μM). (**B**, **C**) Twenty-four hours after the intraventricular injection, TUNEL+ cells (markers of apoptosis) in the dentate gyrus of the hippocampus increased significantly.
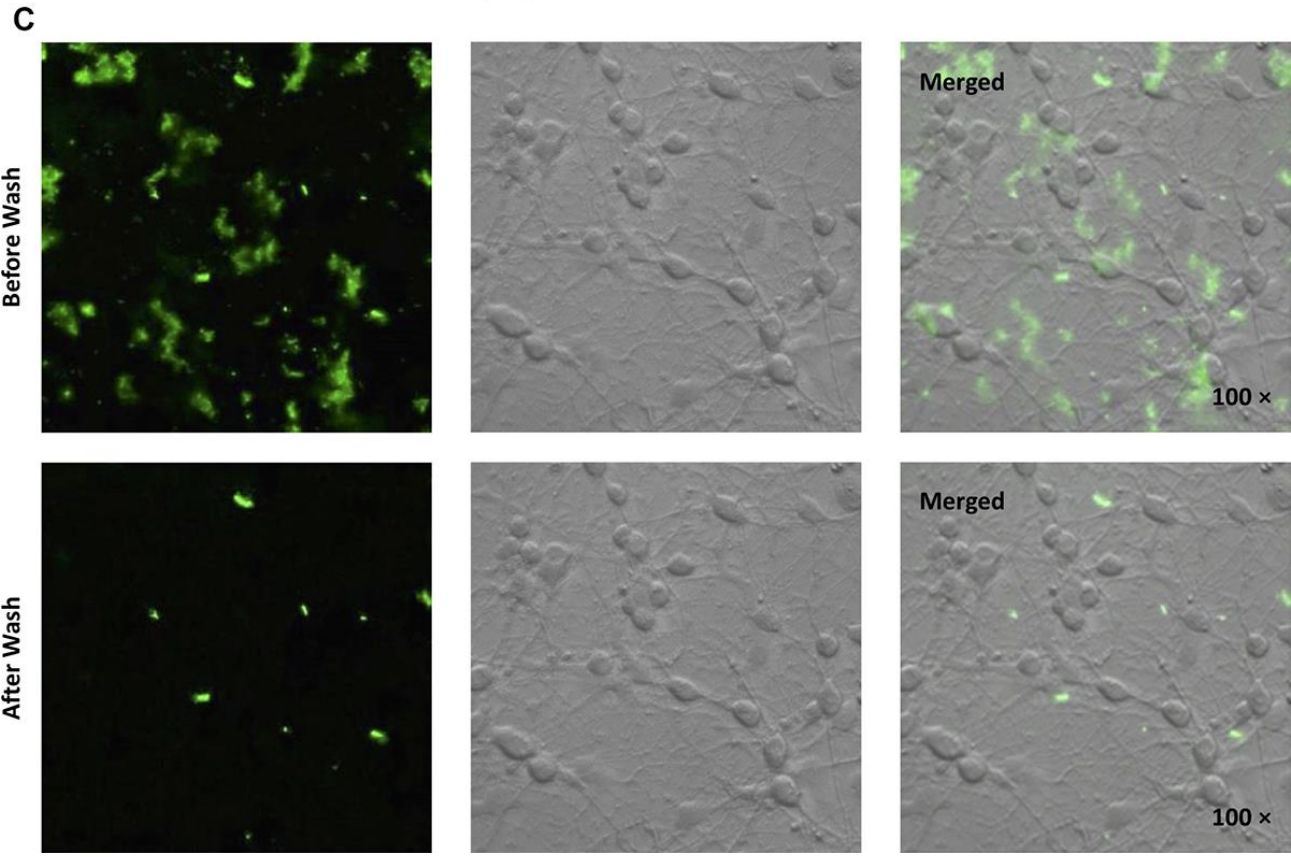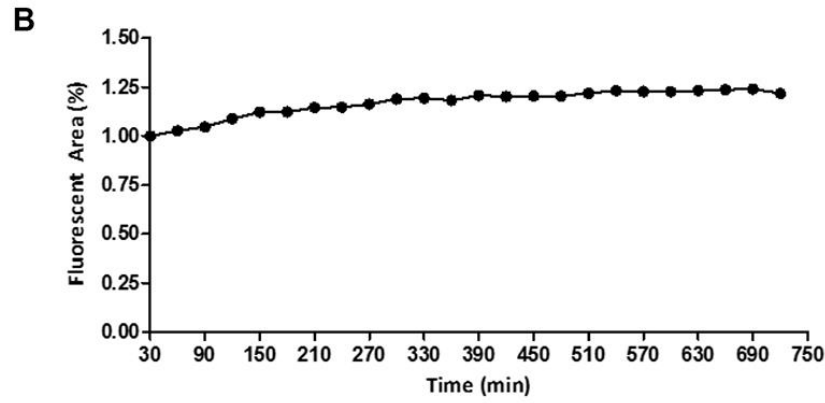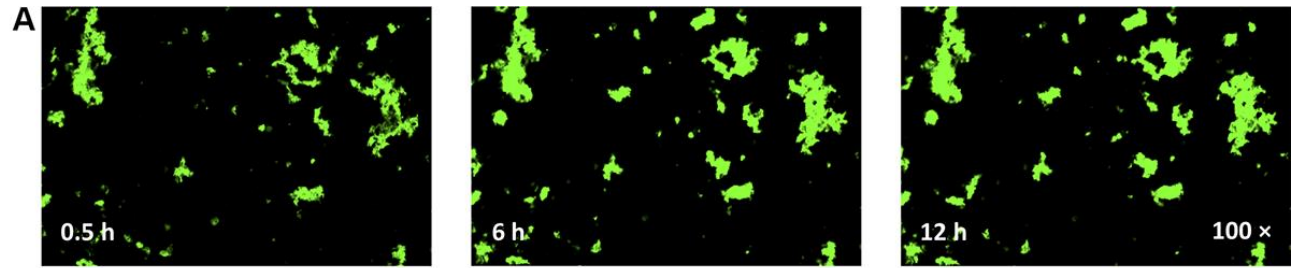
Figure 2. (**A**, **B**) FAM-labeled hAmylin aggregates on the surface of a primary culture of hippocampal neurons, after 30 min of incubation. The fluorescence area of FAM-hAmylin aggregates increased slightly with time (**A**: typical image; **B**: fluorescence area change). (**C**) After the culture dish had been washed and shaken with fresh medium without FAM-hAmylin, the fluorescence of aggregated hAmylin was significantly reduced.
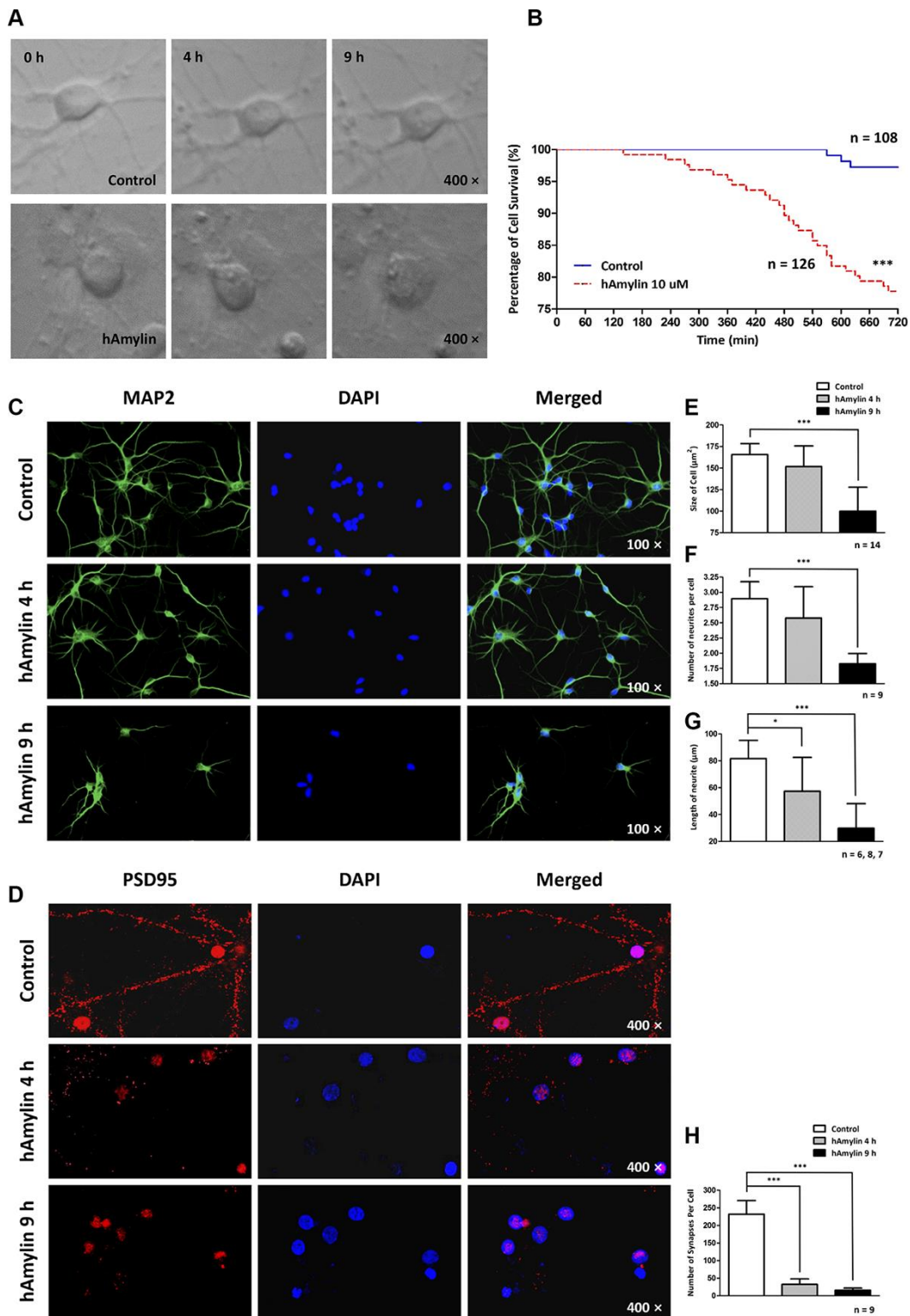
Figure 3. Long-term effects of 10 μM hAmylin on the morphology of hippocampal neurons. (**A**) Typical images of cultured hippocampal neurons were captured in fresh medium with or without 10 μM hAmylin at different time points. (**B**) The survival percentages in the control (n = 108) and 10 μM hAmylin (n = 126) groups. ***p < 0.001 versus control group (Gehan-Breslow-Wilcoxon test). (**C, D**) MAP2 (a neuronal marker) (**C**) and PSD95 (a synapse marker) (**D**) were used to detect morphological changes in neurons at different time points of hAmylin incubation. (**E–H**) Cell size (**E**), neurite length (**G**), neurite number (**F**) and synapse number (**H**) were measured. After the neurons had been incubated for 4 h with 10 μM hAmylin, their synapse numbers (p < 0.001) and neurite lengths (p < 0.05) were significantly reduced. After 9 h of incubation, the cell sizes (p < 0.001) and neurite numbers (p < 0.01) were significantly reduced.

evaluate the integrity of the cell membrane and to determine whether hAmylin damaged the neuronal membrane. Intracellular fluorescence (marked by microtubule-associated protein 2 (MAP2), a neuronal marker) was detected when neurons were incubated with Triton X-100, but was almost invisible when Triton X-100 was replaced with phosphate-buffered saline (PBS). However, when 10 μM hAmylin was used (for 1 min or 30 min) instead of Triton X-100, intracellular MAP2 fluorescence was still observed (Figure 4A and 4B). The percentage of positive cells was 31.01% for 1-min incubation and 35.15% for 30-min incubation (Figure 4C). Intracellular fluorescence of an astrocytic marker (S100) was not clearly detected in astrocytes when 10 μM hAmylin was used instead of Triton X-100 (incubation for 1 min) (Figure 4D). However, when the incubation time with hAmylin was prolonged to 30 min, intracellular fluorescence was observed in 34.65% of astrocytes (Figure 4D–4F). These results indicated that hAmylin disrupts the cell membrane integrity in a Triton-like manner, but requires different amounts of time to destroy different types of cell membranes.

Next, scanning electron microscopy was used to further examine the effects of hAmylin on the stability of the cell membrane. After the cells had been incubated with hAmylin (10 μM, 1 h), the integrity of the plasma membrane was destroyed in both neurons and astrocytes (Figure 5A). Several pores were visible on the surface of the cell membrane, and as the cell structure collapsed, the contours of the nucleus became apparent.

Effects of hAmylin on ROS generation and the mtΔΨ in neurons

ROS generation and changes in oxidation status are important contributors to the membrane impairment caused by β-amyloid proteins in neurons [30–33]. Like β-amyloid, hAmylin enhanced the generation of ROS in neurons when it was applied at a high concentration (10 μM, ***p < 0.001), but not when it was applied at a low concentration (1 μM). In addition, the removal of extracellular calcium had no effect on the ROS generation induced by a high concentration of hAmylin (Figure 5B–5D).

ROS, the natural byproducts of normal respiratory metabolism, are mainly generated by mitochondria. Mitochondria are also particularly vulnerable to oxidative stress. ROS can activate the mitochondrial permeability transition pore (mPTP), which can depolarize the mtΔΨ. JC-1 dye was used to investigate the effects of hAmylin on the mtΔΨ in neurons. The mtΔΨ was significantly reduced by a high concentration of hAmylin (10 μM), but not by a low concentration (1

μM). Although the reduction of the mtΔΨ induced by a high concentration of hAmylin was not suppressed by the removal of extracellular calcium, it was significantly inhibited (***p < 0.001) by the administration of 1 μM cyclosporin A (CsA, an inhibitor of mPTP opening; Figure 5E–5G). However, CsA did not inhibit the increases in [Ca^{2+}]$_i$ (Supplementary Figure 1C and 1D) and ROS levels (Figure 5B and 5C) in response to hAmylin.

DISCUSSION

In the present study, we injected hAmylin directly into the lateral ventricles of mice, which resulted in hippocampal neuronal apoptosis without microglial migration. *In vitro*, a high concentration of hAmylin (10 μM) induced morphological changes in neurons. We assessed the survival, cell size, neurite length, neurite number and synapse number of neurons during their long-term incubation with hAmylin, and found that hAmylin directly impaired neuronal survival and morphology. Moreover, using FAM-hAmylin, we observed significant aggregation of hAmylin on the neuronal membrane. The irreversible aggregation of hAmylin ruptured the cell membrane, generated ROS, reduced the mtΔΨ and eventually induced neuronal death.

Amylin oligomers and plaques have been identified in temporal lobe gray matter from diabetic patients, and amylin deposition has been detected in the blood vessels and brain parenchyma of late-onset Alzheimer's disease patients without clinically apparent diabetes [8]. This suggests that amylin is harmful not only to the pancreas, but also to the central nervous system. However, the absence of amylin transcripts in the human brain indicates that amylin oligomers secreted into the blood from the pancreas are the main source of amylin in the brain [8]. There is no evidence that amylin oligomers can cross the blood-brain barrier, so researchers tend to believe that amylin can only enter the central nervous system from the periphery when the blood-brain barrier is damaged (due to aging, DM2, etc.) [34, 35].

Quasi-spherical Zn^{2+}-β-amyloid-40 oligomers have been reported to irreversibly inhibit spontaneous neuronal activity and cause massive cell death in primary hippocampal neurons [36]. We previously explored the neuronal damage caused by hAmylin oligomers, and found that their cytotoxicity stemmed from their aggregation. This process indirectly activated the TRPV4 channel, thus increasing neuronal [Ca^{2+}]$_i$ levels [14]. However, at the time of that study, we could not explain why amylin did not increase the [Ca^{2+}]$_i$ of astrocytes, which also express TRPV4. Other studies have indicated that hAmylin can form non-selective ion-permeable channels on the surface of the lipid
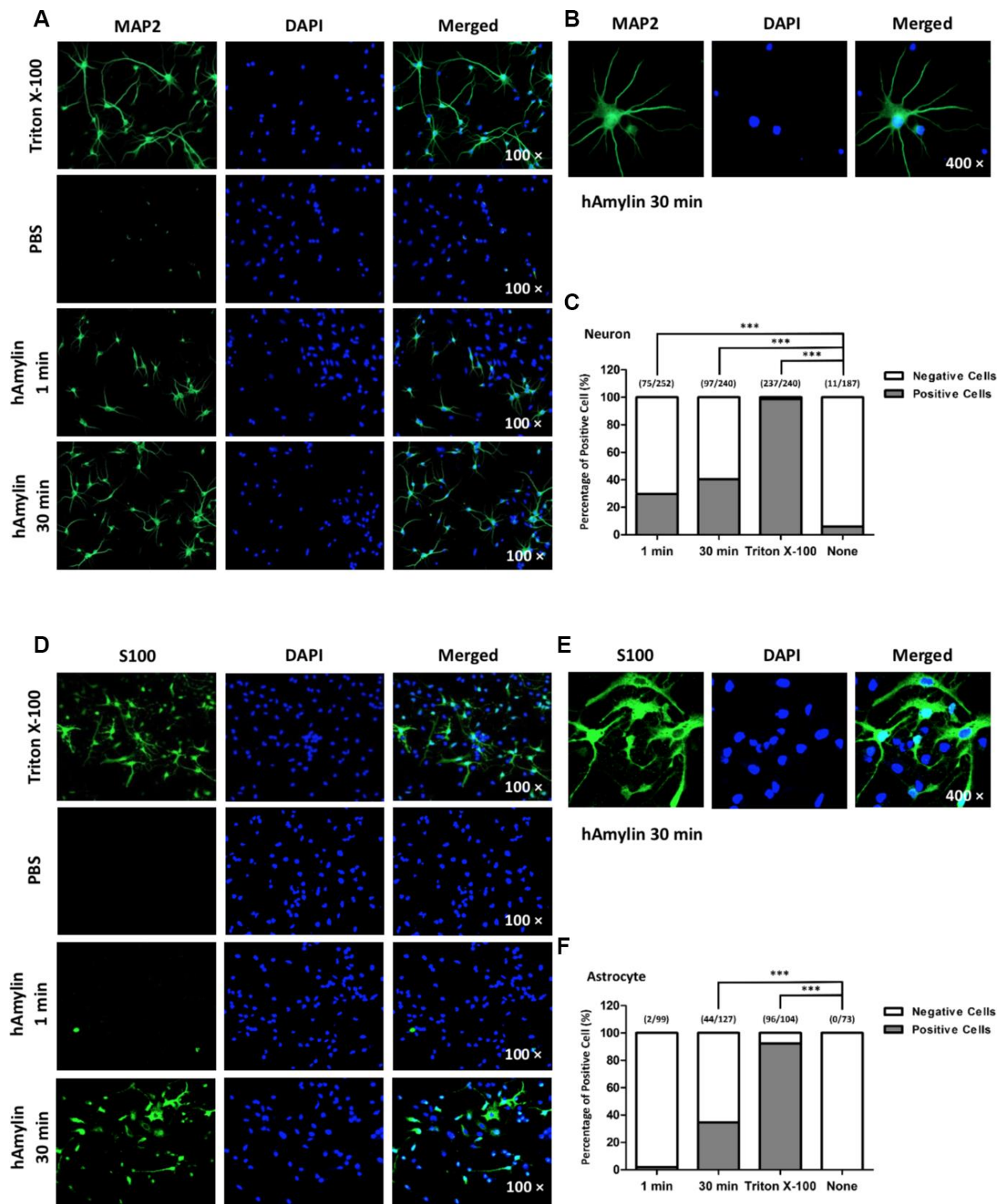
Figure 4. The permeabilization effects of hAmylin on neurons and astrocytes. (**A**, **B**) Neuron-specific fluorescence (MAP2) was observed in neurons after their incubation with Triton X-100. When Triton X-100 was replaced with PBS, intracellular fluorescence was almost invisible. However, when 10 µM hAmylin was used instead of Triton X-100 (incubation for 1 min or 30 min), intracellular fluorescence could still be observed in neurons. (**C**) The percentage of positive cells was 31.01% for 1 min incubation and 35.15% for 30 min incubation. (**D–F**) In contrast, astrocyte-specific fluorescence (S100) was not clearly observed when 10 µM hAmylin was used instead of Triton X-100 (incubation for 1 min). However, when the incubation time was prolonged to 30 min, intracellular fluorescence could be observed (**D**, **E**) in 34.65% of astrocytes (**F**). ***$p < 0.001$ versus PBS group (chi-square test).
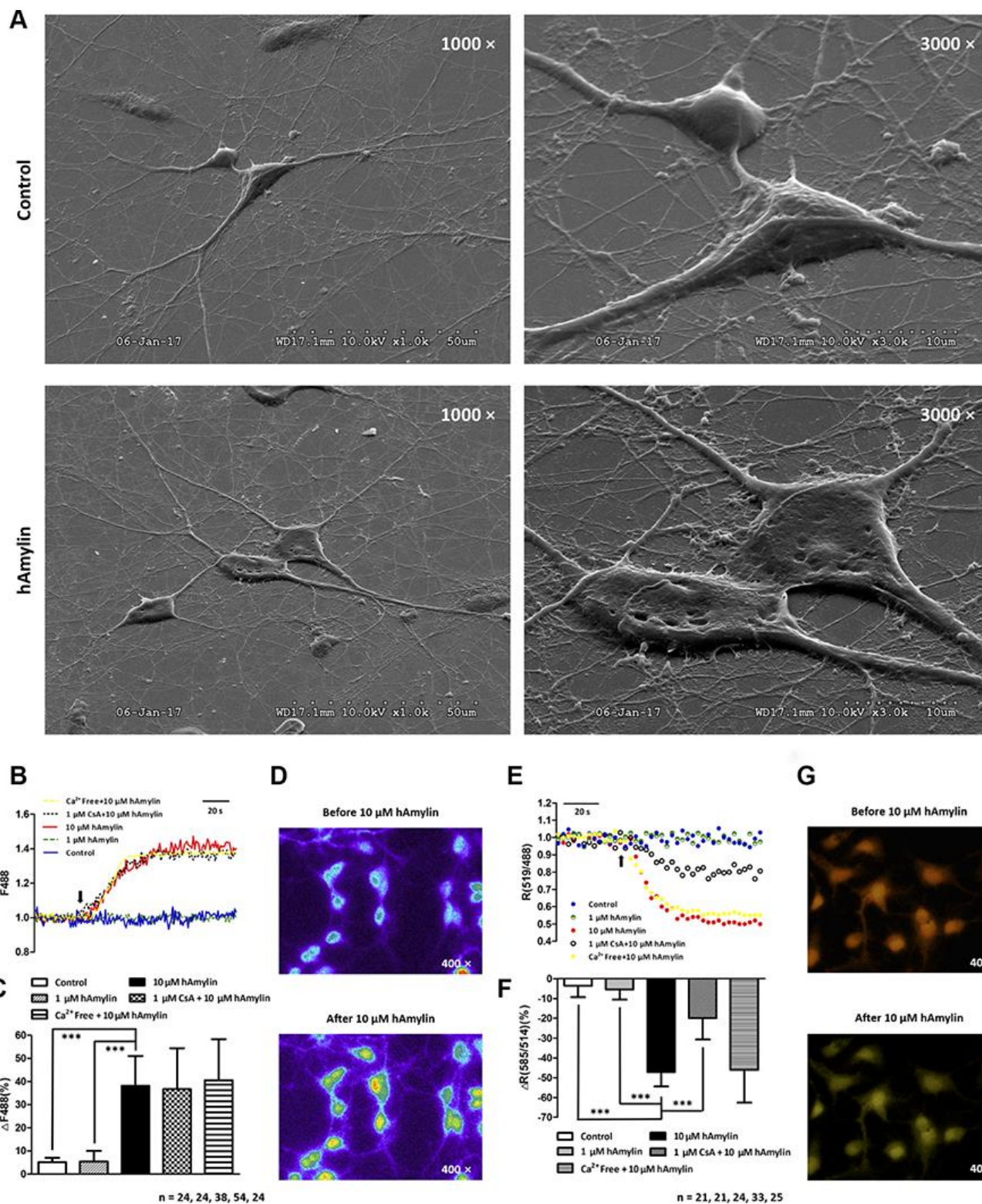
Figure 5. Scanning electron microscopy images of primary cultured hippocampal cells with or without hAmylin (10 μM, 1 h).
(**A**) The plasma membrane was smooth and integral for primary cultured neurons and astrocytes without amylin incubation. After the cells had been treated with hAmylin (10 μM), significant plasma membrane damage was observed on the surface of primary cultured neurons and astrocytes. (**B**) Intracellular ROS generation induced by 10 μM hAmylin was measured in hippocampal neurons labeled with DCFH-DA dye. Representative traces are shown of the effects of 1 μM hAmylin, 10 μM hAmylin, 10 μM hAmylin + 1 μM CsA and 10 μM hAmylin + free Ca^{2+} on ROS generation. (**C**) Significant ROS generation was induced by 10 μM hAmylin, and was not inhibited by 1 μM CsA or free extracellular Ca^{2+}. (**D**) Changes in neuronal DCFH-DA fluorescence before and after 10 μM hAmylin incubation. (**E**) The reduction in the mtΔΨ induced by

10 μM hAmylin was measured in hippocampal neurons labeled with JC-1 dye. Representative traces are shown of the effects of 1 μM hAmylin, 10 μM hAmylin, 10 μM hAmylin + 1 μM CsA and 10 μM hAmylin + free Ca^{2+} on the mtΔΨ. (**F**) Significant mtΔΨ reduction was induced by 10 μM hAmylin and inhibited by 1 μM CsA, but not by free extracellular Ca^{2+}. (**G**) Changes in neuronal JC-1 fluorescence before and after 10 μM hAmylin incubation. ***$p < 0.001$ versus 10 μM hAmylin (one-way ANOVA followed by Bonferroni's post hoc test).

bilayer [12, 37]. Considering that TRPV4 is an ion channel that senses changes in the osmotic pressure of cells [38], we speculated that hAmylin might destroy the integrity of the cell membrane before activating TRPV4.

In this paper, we further explored the damaging effects of amylin oligomers on the cell membrane. In accordance with previous studies, our results indicated that when hAmylin was applied at a high concentration, it aggregated and induced neuronal loss both *in vitro* [14] and *in vivo* [26, 39]. We first demonstrated this by using specific impermeable immunofluorescent antibodies to stain neurons and astrocytes. We replaced the common permeabilization reagent Triton X-100 with hAmylin, and observed neuron-specific fluorescence after 1 min of incubation. However, in the same incubation period, no intracellular fluorescence was detected in astrocytes. When the incubation time was prolonged to 30 min, intracellular fluorescence could be detected in both neurons and astrocytes. In addition, scanning electron microscopy clearly revealed the plasma membrane damage induced by hAmylin. These results indicated that hAmylin damages the cell membrane during its surface aggregation, and that different incubation periods are required for hAmylin to disrupt the membranes of different cell types, with neurons being particularly vulnerable.

β-amyloid can also form pores on the surface of the cell membrane, and the time required for this process correlates with the cholesterol content of the membrane [44]. We speculate that hAmylin and β-amyloid disrupt the cell membrane integrity by similar mechanisms. The membrane cholesterol content is higher in astrocytes than in neurons [45], which may explain why 10 μM hAmylin damaged the neuronal membrane more rapidly than the astrocyte membrane [45]. The non-selective damage to the cell membrane integrity during prolonged incubation with hAmylin suggests that this protein may destroy the membranes of neurons [14, 26, 39], cardiomyocytes [40], pancreatic β-cells [41–43], etc through similar mechanisms. Considering that most DM2 patients have neurological and cardiovascular system complications, we hypothesize that plasma membrane damage caused by hAmylin may be an important contributor to the complications of DM2 patients.

Previous studies have demonstrated that β-amyloid proteins damage the cell membrane by generating large amounts of ROS while aggregating [20, 46, 47]. Similarly, our results revealed that a high concentration of hAmylin significantly increased ROS generation in neurons, while a low concentration of hAmylin (1 μM) did not. ROS, which may contain oxygen free radicals, are highly reactive molecules. ROS are mainly
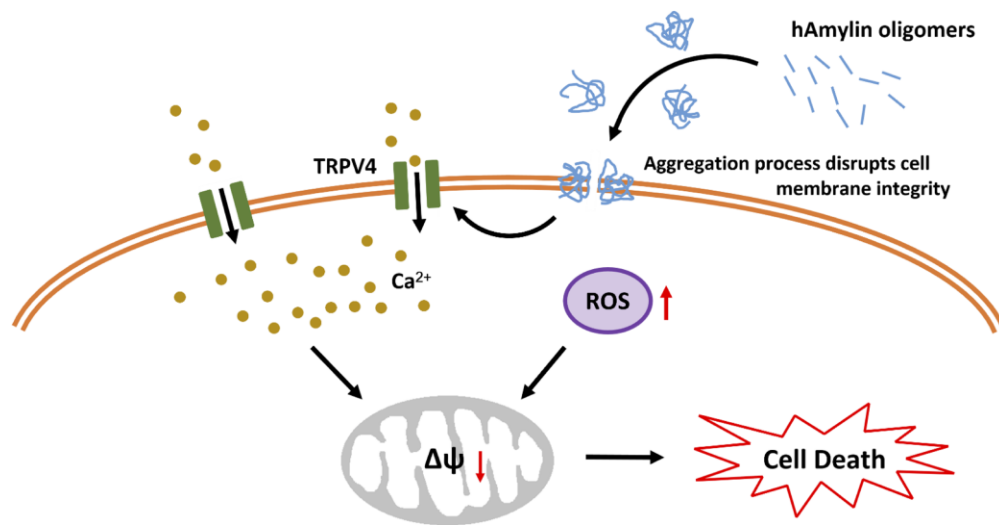
Figure 6. Schematic diagram of hAmylin-induced apoptosis. hAmylin irreversibly aggregates and forms pores on the surface of the cell membrane, thus increasing ROS generation. On the other hand, changes in cellular osmotic pressure activate TRPV4 channels, leading to extracellular calcium ion influx. Increased [Ca^{2+}]$_i$ and ROS levels reduce the mtΔΨ and eventually induce apoptosis.

generated in mitochondria as the byproducts of respiratory metabolism, although they may also be produced in the endoplasmic reticulum, peroxisome, cytosol, plasma membrane and extracellular space [48]. Although we found that hAmylin upregulated ROS production in neurons, further investigation is needed to determine the subcellular site of ROS generation.

Mitochondria are also vulnerable to oxidative stress. In mitochondria, the ROS-triggered release of additional ROS is associated with the opening of the mPTP [49]. The mPTP is located in the inner membrane of the mitochondria, where it regulates the mitochondrial membrane permeability and mtΔΨ. The mtΔΨ is abolished once the mPTP is opened by molecules such as ROS and Ca^{2+}, and this results in cell death [50]. We found that a high concentration of hAmylin significantly reduced the mtΔΨ in neurons. CsA significantly inhibited this reduction of the mtΔΨ, although it did not inhibit the increases in $[Ca^{2+}]_i$ and ROS levels induced by hAmylin. These results indicated that the hAmylin-induced reduction of the mtΔΨ was a downstream response to ROS generation (Figure 6). Increased $[Ca^{2+}]_i$ and ROS levels were probably the underlying factors leading to the abolished mtΔΨ and the initiation of neuronal death.

In conclusion, our study has provided evidence that hAmylin irreversibly aggregates on the surface of the cell membrane and disrupts its integrity. This process is accompanied by increased intracellular ROS generation. On the other hand, previous work has indicated that changes in the osmotic pressure of cells activate TRPV4 channels, leading to the influx of extracellular calcium ions. Increased $[Ca^{2+}]_i$ and ROS levels activate the mPTP, which subsequently reduces the mtΔΨ and induces apoptosis. Our results also demonstrate that hAmylin induces non-selective cell membrane damage, although neuronal cell membranes are more vulnerable to hAmylin than astrocyte cell membranes. Thus, inhibiting hAmylin aggregation may be a new target for treating associated diseases.

MATERIALS AND METHODS

Animals and primary hippocampal cultures

Pregnant adult Sprague-Dawley rats (RRID: MGI:5651135) and adult Kunming laboratory mice (RRID: MGI:5651867) were purchased from the Hebei Laboratory Animal Center. All animal care and experimental procedures complied with the regulations of the Animal Care and Management Committee of the Second Hospital of Hebei Medical University (permit No. HMUSHC-130318) and the Animal Research: Reporting *In Vivo* Experiments (ARRIVE) guidelines for subsequent experiments [51, 52].

Primary cultures of hippocampal neurons and astrocytes were prepared from Sprague-Dawley rats according to previously described methods [53].

Main chemicals

Dulbecco's modified Eagle's medium, fetal bovine serum, fura-2-acetoxy-methyl ester, 4-(2-hydroxyethyl)-1-piperazineethanesulfonic acid (HEPES), glucose and PBS were obtained from Invitrogen (USA). Penicillin and streptomycin, NaCl, KCl, $MgCl_2$, $CaCl_2$ and glucose were purchased from Sigma (USA). CsA, JC-1, an In Situ BrdU-Red DNA Fragmentation (TUNEL) Assay Kit (ab66110), anti-TMEM119 (ab209064), anti-Iba1 (ab153696), anti-S100 (ab868), anti-MAP2 (ab11267) and anti-PSD95 (ab18258) were obtained from Abcam (USA). Donkey anti-mouse IgG (Cat#A-21202, Alexa Fluor 488), donkey anti-rabbit IgG (Cat#A-21206, Alexa Fluor 488) and donkey anti-rabbit IgG (Cat#A-21207, Alexa Fluor 594) were purchased from Thermo Fisher (USA). Finally, 2',7'-dichlorofluorescin-diacetate (DCFH-DA) was purchased from Beyotime (China).

hAmylin (Tocris, UK) was dissolved to 500 μM in sterile water and immediately diluted with HEPES buffer (see calcium imaging methods) to a final concentration of 1 or 10 μM at room temperature. FAM-hAmylin was purchased from Shanghai Science Peptide Biological Technology Co., Ltd. (China). The sequence of hAmylin is KCNTATCATQRLANFL VHSSNNFGAILSSTNVGSNTY (Modifications: Tyr-37 = C-terminal amide, Disulfide bridge between 2 - 7).

Lateral ventricle injection

Six adult male Kunming mice were randomly divided into two groups. The mice were subjected to isoflurane inhalation anesthesia (initial concentration 3%, maintenance concentration 1.5%). Their teeth were buckled onto a tooth bar and their noses were fastened with a clip. Ear bars were inserted into the external ear canals of both ears so that the scales of the two bars were consistent. After the head was fixed, the height of the body was adjusted so that the body and head were horizontal. The head skin was disinfected with iodine volt cotton swabs. A midline incision was made at the top of the head to expose the bregma, and a marker was used to denote a point 1 mm to the right and 0.22 mm to the rear of the bregma at a needle depth of 2.3 mm. An electric skull drill was used to drill a small hole with a diameter of about 0.5 mm at the marked location, and a fixed micro-injector was slowly inserted to the specified depth. Then, 5 μL of 10 μM hAmylin was injected with a micro-pump at a speed of 1 μL/min. The mice in the control group were injected with saline. After the injection, the mice were monitored for 5 min to ensure that the entire drug dose in the micro-

injector had entered the lateral ventricle. The micro-injector was extracted over a period of 5 min, and the incision was sutured. The mice were sacrificed 24 h after the injection, and three brain slices near the pinhole were collected. To avoid left and right confusion, we only retained right brain tissue during sampling.

Immunochemistry

Brains were collected after the mice had been perfused with 0.9% NaCl followed by 4% paraformaldehyde. Immunofluorescence analysis of the hippocampus was conducted according to previously described methods [54]. Cerebral sections were cut from frozen blocks with a sliding microtome at a thickness of 30 μm. Fixed brain slices were permeabilized with 0.5% Triton X-100 in PBS for 20 min at room temperature and then blocked with 10% donkey serum for 30 min. The slices were incubated at 4°C overnight with the following primary antibodies: anti-TMEM119 (1:200), anti-Iba1 (1:200), anti-S100 (1:200), anti-MAP2 (1:200) and anti-PSD95 (1:200). After being washed with PBS three times, the slices were incubated for 1 h at 37 °C with secondary antibodies (1:100), and then were washed in PBS for 5 min three times. Cell nuclei were visualized with 4',6-diamidino-2-phenylindole (DAPI) in PBS for 10 min at room temperature. A laser scanning confocal microscope (Olympus BX61+DP71, Japan) was used to observe immunofluorescence.

For the primary cultured hippocampal cell analysis, neurons or astrocytes were applied to coverslips, washed with PBS three times and then fixed with 4% paraformaldehyde in PBS for 15 min at room temperature. The cells were then permeabilized with 0.5% Triton X-100 in PBS for 20 min at room temperature. The subsequent steps of immunochemistry were the same as those described above for the brain slices. In the fluorescence experiments to assess whether hAmylin disrupted the integrity of the cell membrane, we incubated the cells with 10 μM hAmylin or PBS instead of Triton X-100 (1 min or 30 min), but the other steps were the same.

TUNEL staining was performed according to the In situ BrdU-Red DNA Fragmentation (TUNEL) Assay Kit instructions. The proportion of apoptotic cells was calculated as the number of TUNEL^{+} cells / the number of DAPI^{+} cells × 100%.

Scanning electron microscopy

The specimen was fixed with 2.5% glutaraldehyde in phosphate buffer (pH 7.0) for more than 4 h, and then was washed three times in phosphate buffer. Next, the specimen was post-fixed with 1% OsO_4 in phosphate buffer (pH 7.0) for 1 h, and was subsequently washed

three times in phosphate buffer. The specimen was dehydrated in a graded series of ethanol solutions (30%, 50%, 70%, 80%, 90%, 95% and 100%) for about 15 to 20 min at each step. Then, it was transferred to a mixture of ethanol and isoamyl acetate (v:v = 1:1) for about 30 min, and transferred to pure isoamyl acetate for about 1 h. The specimen was then dehydrated in a Hitachi Model HCP-2 critical point dryer with liquid CO_2. The dehydrated specimen was coated with gold-palladium and observed with an S-3500N scanning electron microscope (Hitachi, Japan).

Live cell imaging

To investigate the long-term effects of hAmylin on neurons, we used a large BL incubator (PeCon, Germany) with a Leica microscope (Leica, #11600198) to image living cells at 37 °C with 5% CO_2. Neurons treated with FAM-labeled hAmylin were imaged every 30 min for 12 h. In the cell survival experiment with 10 μM hAmylin, images were taken every 10 min for 12 h.

Calcium imaging

Calcium imaging was performed as described previously [14]. Fura-2-acetoxymethyl ester (2 μM) was loaded into cultured rat hippocampal neurons for 20 min at 37 °C. After the loading step, the hippocampal neurons were washed with HEPES buffer to remove the extracellular dye, the cells were observed through an inverted microscope (Leica DMI3000), and images were captured with a ratiometric imaging system (Metafluor, CA) at room temperature. The calcium signals were generated using 340 and 380 nm excitation (monochromator, Polychrome V, TILL Photonics, NY, USA) and imaged with a cooled electron multiplying charge-coupled device camera (Andor, Germany). The HEPES buffer contained 145 mM NaCl, 3 mM KCl, 2 mM $MgCl_2$, 2 mM $CaCl_2$, 10 mM glucose and 10 mM HEPES (adjusted to pH 7.4 with NaOH). The 340/380-nm fluorescence intensity ratio was calculated as previously described [14]. All agents for calcium imaging were dissolved in HEPES buffer. The drugs were applied locally to the cells through an eight-channel pressure-controlled drug application system (ALA Scientific, USA).

Measurement of ROS generation

As described in our previously published paper [53], we assessed the intracellular ROS generation induced by the drug intervention by measuring fluorescence intensity using DCFH-DA. Hippocampal neurons were loaded with DCFH-DA in the dark at 37 °C for 20 min, and then were washed and perfused with HEPES buffer according to the same method used for calcium

imaging. ROS signals were excited at 488 nm on a Leica DMI3000B microscope (Leica Microsystems Inc.) equipped with a ratiometric imaging system, and images were recorded at 1-s intervals using a cooled electron multiplying charge-coupled device camera (Andor). ROS generation, as indicated by the fluorescence intensity at 488 nm in cells loaded with DCFH-DA, was calculated as follows: ROS generation (488 nm) = [(P488 nm – B488 nm) / B488 nm] × 100%, where P488 nm is the peak fluorescence intensity after the intervention, and B488 nm is the baseline fluorescence intensity before the intervention.

Measurement of the mitochondrial membrane potential

The mtΔΨ was measured as previously described [53]. JC-1 dye (10 μg/mL, 20 min, 37 °C) was loaded into hippocampal neurons, and images were captured on a Leica DMi8 two-photon confocal laser scanning microscope (Leica Microsystems Inc., Germany). Wavelengths of 488 and 519 nm were used for the mtΔΨ signals, and the ratio of 519/488 nm represented the change in the mtΔΨ.

Statistical analysis

Data are presented as the mean ± standard deviation. A Gehan-Breslow-Wilcoxon test was used to analyze the neuronal survival curve, and a chi-square test was used to evaluate differences in the percentage of positive cells between the groups. One-way analysis of variance (ANOVA) followed by Bonferroni's post hoc test was used to compare the ROS levels and mtΔΨ of the groups. Differences between pre- and post-treatment values in the same cell type were assessed with a paired t test. A p value less than 0.05 was considered statistically significant. Data were analyzed with GraphPad Prism software (v. 5.00, USA) and SPSS software (v. 20.0, USA). The sample sizes were based on previous international research experience and published papers. No randomization methods were used in this study. The experimenters were not blinded to the conditions of the study. Our experiments did not involve any missing data, lost data or excluded data.

Abbreviations

CsA: Cyclosporin A; DM2: type 2 diabetes mellitus; FAM: fluorescein amidite; hAmylin: human amylin; Iba1: ionized calcium binding adaptor molecule 1; MAP2: microtubule-associated protein 2; mPTP: mitochondrial permeability transition pore; PBS: phosphate-buffered saline; ROS: reactive oxygen species; TMEM199: transmembrane protein 199; TRPV4: transient receptor potential vanilloid 4 channels.

AUTHOR CONTRIBUTIONS

WZ designed the research; LK and WZ designed the experiments; NZ, YX, HM, LH, YY and WB performed the experiments; NZ, YX, ZJ and HM analyzed the data; ZJ, XZ, RZ, LK and WZ prepared the manuscript. All authors approved the final version of the manuscript.

CONFLICTS OF INTEREST

The authors declare that they have no conflicts of interest with the contents of this article.

FUNDING

REFERENCES

1. Mattson MP. Pathways towards and away from alzheimer's disease. Nature. 2004; 430:631–39.
   https://doi.org/10.1038/nature02621
   PMID:15295589

2. Halim M, Halim A. The effects of inflammation, aging and oxidative stress on the pathogenesis of diabetes mellitus (Type 2 diabetes). Diabetes Metab Syndr. 2019; 13 :1165–72.
   https://doi.org/10.1016/j.dsx.2019.01.040
   PMID:31336460

3. Janson J, Laedtke T, Parisi JE, O'Brien P, Petersen RC, Butler PC. Increased risk of type 2 diabetes in alzheimer disease. Diabetes. 2004; 53:474–81.
   https://doi.org/10.2337/diabetes.53.2.474
   PMID:14747300

4. Press M, Jung T, König J, Grune T, Höhn A. Protein aggregates and proteostasis in aging: amylin and β-cell function. Mech Ageing Dev. 2019; 177:46–54.
   https://doi.org/10.1016/j.mad.2018.03.010
   PMID:29580826

5. Glenner GG, Eanes ED, Wiley CA. Amyloid fibrils formed from a segment of the pancreatic islet

amyloid protein. Biochem Biophys Res Commun. 1988; 155:608–14.
https://doi.org/10.1016/s0006-291x(88)80538-2
PMID:3048259

6. May PC, Boggs LN, Fuson KS. Neurotoxicity of human amylin in rat primary hippocampal cultures: similarity to alzheimer's disease amyloid-beta neurotoxicity. J Neurochem. 1993; 61:2330–33.
https://doi.org/10.1111/j.1471-4159.1993.tb07480.x
PMID:8245987

7. Götz J, Lim YA, Eckert A. Lessons from two prevalent amyloidoses-what amylin and Aβ have in common. Front Aging Neurosci. 2013; 5:38.
https://doi.org/10.3389/fnagi.2013.00038
PMID:23964237

8. Jackson K, Barisone GA, Diaz E, Jin LW, DeCarli C, Despa F. Amylin deposition in the brain: a second amyloid in alzheimer disease? Ann Neurol. 2013; 74:517–26.
https://doi.org/10.1002/ana.23956 PMID:23794448

9. Pannuzzo M, Raudino A, Milardi D, La Rosa C, Karttunen M. A-helical structures drive early stages of self-assembly of amyloidogenic amyloid polypeptide aggregate formation in membranes. Sci Rep. 2013; 3:2781.
https://doi.org/10.1038/srep02781
PMID:24071712

10. Brender JR, Lee EL, Cavitt MA, Gafni A, Steel DG, Ramamoorthy A. Amyloid fiber formation and membrane disruption are separate processes localized in two distinct regions of IAPP, the type-2-diabetes-related peptide. J Am Chem Soc. 2008; 130:6424–29.
https://doi.org/10.1021/ja710484d
PMID:18444645

11. Brender JR, Salamekh S, Ramamoorthy A. Membrane disruption and early events in the aggregation of the diabetes related peptide IAPP from a molecular perspective. Acc Chem Res. 2012; 45:454–62.
https://doi.org/10.1021/ar200189b
PMID:21942864

12. Mirzabekov TA, Lin MC, Kagan BL. Pore formation by the cytotoxic islet amyloid peptide amylin. J Biol Chem. 1996; 271:1988–92.
https://doi.org/10.1074/jbc.271.4.1988
PMID:8567648

13. Westermark P, Engström U, Johnson KH, Westermark GT, Betsholtz C. Islet amyloid polypeptide: pinpointing amino acid residues linked to amyloid fibril formation. Proc Natl Acad Sci USA. 1990; 87:5036–40.
https://doi.org/10.1073/pnas.87.13.5036
PMID:2195544

14. Zhang N, Yang S, Wang C, Zhang J, Huo L, Cheng Y, Wang C, Jia Z, Ren L, Kang L, Zhang W. Multiple target

of hAmylin on rat primary hippocampal neurons. Neuropharmacology. 2017; 113:241–51.
https://doi.org/10.1016/j.neuropharm.2016.07.008
PMID:27743934

15. Betsholtz C, Christmansson L, Engström U, Rorsman F, Svensson V, Johnson KH, Westermark P. Sequence divergence in a specific region of islet amyloid polypeptide (IAPP) explains differences in islet amyloid formation between species. FEBS Lett. 1989; 251:261–64.
https://doi.org/10.1016/0014-5793(89)81467-x
PMID:2666169

16. Potter KJ, Scrocchi LA, Warnock GL, Ao Z, Younker MA, Rosenberg L, Lipsett M, Verchere CB, Fraser PE. Amyloid inhibitors enhance survival of cultured human islets. Biochim Biophys Acta. 2009; 1790:566–74.
https://doi.org/10.1016/j.bbagen.2009.02.013
PMID:19264107

17. Sciacca MF, Milardi D, Messina GM, Marletta G, Brender JR, Ramamoorthy A, La Rosa C. Cations as switches of amyloid-mediated membrane disruption mechanisms: calcium and IAPP. Biophys J. 2013; 104:173–84.
https://doi.org/10.1016/j.bpj.2012.11.3811
PMID:23332070

18. Last NB, Rhoades E, Miranker AD. Islet amyloid polypeptide demonstrates a persistent capacity to disrupt membrane integrity. Proc Natl Acad Sci USA. 2011; 108:9460–65.
https://doi.org/10.1073/pnas.1102356108
PMID:21606325

19. Kumar S, Paul A, Kalita S, Ghosh AK, Mandal B, Mondal AC. Protective effects of β-sheet breaker α/β-hybrid peptide against amyloid β-induced neuronal apoptosis in vitro. Chem Biol Drug Des. 2017; 89:888–900.
https://doi.org/10.1111/cbdd.12912
PMID:27995757

20. Wang Y, Miao Y, Mir AZ, Cheng L, Wang L, Zhao L, Cui Q, Zhao W, Wang H. Inhibition of beta-amyloid-induced neurotoxicity by pinocembrin through Nrf2/HO-1 pathway in SH-SY5Y cells. J Neurol Sci. 2016; 368:223–30.
https://doi.org/10.1016/j.jns.2016.07.010
PMID:27538638

21. Casas S, Novials A, Reimann F, Gomis R, Gribble FM. Calcium elevation in mouse pancreatic beta cells evoked by extracellular human islet amyloid polypeptide involves activation of the mechanosensitive ion channel TRPV4. Diabetologia. 2008; 51:2252–62.
https://doi.org/10.1007/s00125-008-1111-z
PMID:18751967

22. Everaerts W, Nilius B, Owsianik G. The vanilloid transient receptor potential channel TRPV4: from structure to disease. Prog Biophys Mol Biol. 2010; 103:2–17.
https://doi.org/10.1016/j.pbiomolbio.2009.10.002
PMID:19835908

23. Gu Y, Gu C. Physiological and pathological functions of mechanosensitive ion channels. Mol Neurobiol. 2014; 50:339–47.
https://doi.org/10.1007/s12035-014-8654-4
PMID:24532247

24. Fawver JN, Ghiwot Y, Koola C, Carrera W, Rodriguez-Rivera J, Hernandez C, Dineley KT, Kong Y, Li J, Jhamandas J, Perry G, Murray IV. Islet amyloid polypeptide (IAPP): a second amyloid in alzheimer's disease. Curr Alzheimer Res. 2014; 11:928–40.
https://doi.org/10.2174/1567205011666141107124538
PMID:25387341

25. Oskarsson ME, Paulsson JF, Schultz SW, Ingelsson M, Westermark P, Westermark GT. In vivo seeding and cross-seeding of localized amyloidosis: a molecular link between type 2 diabetes and alzheimer disease. Am J Pathol. 2015; 185:834–46.
https://doi.org/10.1016/j.ajpath.2014.11.016
PMID:25700985

26. Srodulski S, Sharma S, Bachstetter AB, Brelsfoard JM, Pascual C, Xie XS, Saatman KE, Van Eldik LJ, Despa F. Neuroinflammation and neurologic deficits in diabetes linked to brain accumulation of amylin. Mol Neurodegener. 2014; 9:30.
https://doi.org/10.1186/1750-1326-9-30
PMID:25149184

27. Tucker HM, Rydel RE, Wright S, Estus S. Human amylin induces "apoptotic" pattern of gene expression concomitant with cortical neuronal apoptosis. J Neurochem. 1998; 71:506–16.
https://doi.org/10.1046/j.1471-4159.1998.71020506.x
PMID:9681440

28. Doré S, Kar S, Quirion R. Insulin-like growth factor I protects and rescues hippocampal neurons against beta-amyloid- and human amylin-induced toxicity. Proc Natl Acad Sci USA. 1997; 94:4772–77.
https://doi.org/10.1073/pnas.94.9.4772
PMID:9114067

29. Mazziotti M, Perlmutter DH. Resistance to the apoptotic effect of aggregated amyloid-beta peptide in several different cell types including neuronal- and hepatoma-derived cell lines. Biochem J. 1998; 332:517–24.
https://doi.org/10.1042/bj3320517 PMID:9601082

30. Deshpande A, Mina E, Glabe C, Busciglio J. Different conformations of amyloid beta induce neurotoxicity by distinct mechanisms in human cortical neurons. J Neurosci. 2006; 26:6011–18.
https://doi.org/10.1523/JNEUROSCI.1189-06.2006
PMID:16738244

31. Forloni G, Artuso V, La Vitola P, Balducci C. Oligomeropathies and pathogenesis of alzheimer and parkinson's diseases. Mov Disord. 2016; 31:771–81.
https://doi.org/10.1002/mds.26624
PMID:27030592

32. Butterfield SM, Lashuel HA. Amyloidogenic protein-membrane interactions: mechanistic insight from model systems. Angew Chem Int Ed Engl. 2010; 49:5628–54.
https://doi.org/10.1002/anie.200906670
PMID:20623810

33. Castegna A, Lauderback CM, Mohmmad-Abdul H, Butterfield DA. Modulation of phospholipid asymmetry in synaptosomal membranes by the lipid peroxidation products, 4-hydroxynonenal and acrolein: implications for alzheimer's disease. Brain Res. 2004; 1004:193–97.
https://doi.org/10.1016/j.brainres.2004.01.036
PMID:15033435

34. Montagne A, Barnes SR, Sweeney MD, Halliday MR, Sagare AP, Zhao Z, Toga AW, Jacobs RE, Liu CY, Amezcua L, Harrington MG, Chui HC, Law M, Zlokovic BV. Blood-brain barrier breakdown in the aging human hippocampus. Neuron. 2015; 85:296–302.
https://doi.org/10.1016/j.neuron.2014.12.032
PMID:25611508

35. Prasad S, Sajja RK, Naik P, Cucullo L. Diabetes mellitus and blood-brain barrier dysfunction: an overview. J Pharmacovigil. 2014; 2:125.
https://doi.org/10.4172/2329-6887.1000125
PMID:25632404

36. Solomonov I, Korkotian E, Born B, Feldman Y, Bitler A, Rahimi F, Li H, Bitan G, Sagi I. Zn2+-Aβ40 complexes form metastable quasi-spherical oligomers that are cytotoxic to cultured hippocampal neurons. J Biol Chem. 2012; 287:20555–64.
https://doi.org/10.1074/jbc.M112.344036
PMID:22528492

37. Zhao J, Luo Y, Jang H, Yu X, Wei G, Nussinov R, Zheng J. Probing ion channel activity of human islet amyloid polypeptide (Amylin). Biochim Biophys Acta. 2012; 1818:3121–30.
https://doi.org/10.1016/j.bbamem.2012.08.012
PMID:22935354

38. Kanju P, Liedtke W. Pleiotropic function of TRPV4 ion channels in the central nervous system. Exp Physiol. 2016; 101:1472–76.
https://doi.org/10.1113/EP085790
PMID:27701788

39. Verma N, Ly H, Liu M, Chen J, Zhu H, Chow M, Hersh LB, Despa F. Intraneuronal amylin deposition, peroxidative membrane injury and increased IL-1β synthesis in brains of alzheimer's disease patients with type-2 diabetes and in diabetic HIP rats. J Alzheimers Dis. 2016; 53:259–72.
https://doi.org/10.3233/JAD-160047
PMID:27163815

40. Despa S, Margulies KB, Chen L, Knowlton AA, Havel PJ, Taegtmeyer H, Bers DM, Despa F. Hyperamylinemia contributes to cardiac dysfunction in obesity and diabetes: a study in humans and rats. Circ Res. 2012; 110:598–608.
https://doi.org/10.1161/CIRCRESAHA.111.258285
PMID:22275486

41. Cao P, Abedini A, Wang H, Tu LH, Zhang X, Schmidt AM, Raleigh DP. Islet amyloid polypeptide toxicity and membrane interactions. Proc Natl Acad Sci USA. 2013; 110:19279–84.
https://doi.org/10.1073/pnas.1305517110
PMID:24218607

42. Zhang S, Liu H, Chuang CL, Li X, Au M, Zhang L, Phillips AR, Scott DW, Cooper GJ. The pathogenic mechanism of diabetes varies with the degree of overexpression and oligomerization of human amylin in the pancreatic islet β cells. FASEB J. 2014; 28:5083–96.
https://doi.org/10.1096/fj.14-251744
PMID:25138158

43. Singh S, Trikha S, Bhowmick DC, Sarkar AA, Jeremic AM. Role of cholesterol and phospholipids in amylin misfolding, aggregation and etiology of islet amyloidosis. Adv Exp Med Biol. 2015; 855:95–116.
https://doi.org/10.1007/978-3-319-17344-3_4
PMID:26149927

44. Arispe N, Doh M. Plasma membrane cholesterol controls the cytotoxicity of alzheimer's disease AbetaP (1-40) and (1-42) peptides. FASEB J. 2002; 16:1526–36.
https://doi.org/10.1096/fj.02-0829com
PMID:12374775

45. Abramov AY, Ionov M, Pavlov E, Duchen MR. Membrane cholesterol content plays a key role in the neurotoxicity of β-amyloid: implications for alzheimer's disease. Aging Cell. 2011; 10:595–603.
https://doi.org/10.1111/j.1474-9726.2011.00685.x
PMID:21332922

46. Zhao Y, Zhao B. Oxidative stress and the pathogenesis of alzheimer's disease. Oxid Med Cell Longev. 2013; 2013:316523.
https://doi.org/10.1155/2013/316523
PMID:23983897

47. Selfridge JE, E L, Lu J, Swerdlow RH. Role of mitochondrial homeostasis and dynamics in alzheimer's disease. Neurobiol Dis. 2013; 51:3–12.
https://doi.org/10.1016/j.nbd.2011.12.057
PMID:22266017

48. Di Meo S, Reed TT, Venditti P, Victor VM. Role of ROS and RNS sources in physiological and pathological conditions. Oxid Med Cell Longev. 2016; 2016:1245049.
https://doi.org/10.1155/2016/1245049
PMID:27478531

49. Zorov DB, Juhaszova M, Sollott SJ. Mitochondrial reactive oxygen species (ROS) and ROS-induced ROS release. Physiol Rev. 2014; 94:909–50.
https://doi.org/10.1152/physrev.00026.2013
PMID:24987008

50. Rottenberg H, Hoek JB. The path from mitochondrial ROS to aging runs through the mitochondrial permeability transition pore. Aging Cell. 2017; 16:943–55.
https://doi.org/10.1111/acel.12650 PMID:28758328

51. Kilkenny C, Browne W, Cuthill IC, Emerson M, Altman DG, and NC3Rs Reporting Guidelines Working Group. Animal research: reporting in vivo experiments: the ARRIVE guidelines. Br J Pharmacol. 2010; 160:1577–79.
https://doi.org/10.1111/j.1476-5381.2010.00872.x
PMID:20649561

52. McGrath JC, Drummond GB, McLachlan EM, Kilkenny C, Wainwright CL. Guidelines for reporting experiments involving animals: the ARRIVE guidelines. Br J Pharmacol. 2010; 160:1573–76.
https://doi.org/10.1111/j.1476-5381.2010.00873.x
PMID:20649560

53. Xing Y, Zhang N, Zhang W, Ren LM. Bupivacaine indirectly potentiates glutamate-induced intracellular calcium signaling in rat hippocampal neurons by impairing mitochondrial function in cocultured astrocytes. Anesthesiology. 2018; 128:539–54.
https://doi.org/10.1097/ALN.0000000000002003
PMID:29232206

54. Zhang N, Zhang X, Liu X, Wang H, Xue J, Yu J, Kang N, Wang X. Chrysophanol inhibits NALP3 inflammasome activation and ameliorates cerebral ischemia/reperfusion in mice. Mediators Inflamm. 2014; 2014:370530.
https://doi.org/10.1155/2014/370530
PMID:24876671

SUPPLEMENTARY MATERIALS

Supplementary Figure
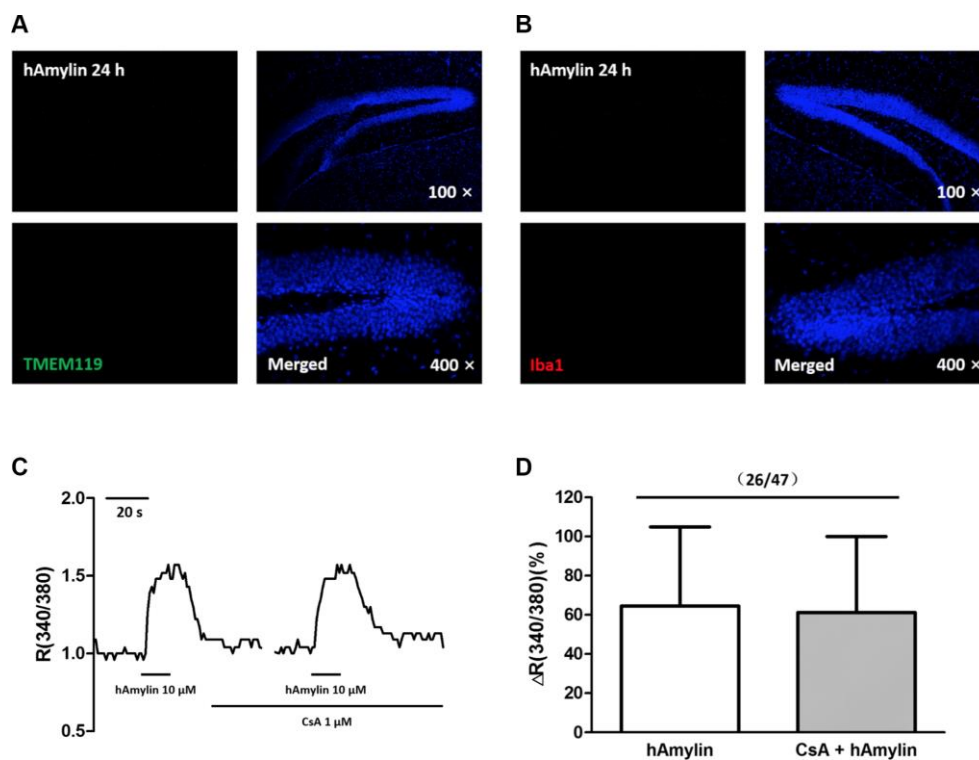
Supplementary Figure 1. (**A**, **B**) Twenty-four hours after hAmylin was injected into the lateral ventricle, no fluorescence of TMEM199 (microglial labeling) (**A**) or Iba1 (microglial and macrophage labeling) (**B**) was observed in the hippocampal dentate gyrus. (**C**) Typical traces showing the effects of 10 μM hAmylin and 10 μM hAmylin + 1 μM CsA on $[Ca^{2+}]_i$ in hippocampal neurons. (**D**) CsA did not change the hAmylin-induced increase in $[Ca^{2+}]_i$. The ratio in parentheses is the positive percentage of neurons responding to hAmylin. p > 0.05 versus the response before CsA treatment (paired t test).